The University of
Nottingham

UNITED KINGDOM · CHINA · MALAYSIA

Leighton, Andrew D. and Hart, Malcolm B. and Smart, Christopher W. and Leng, Melanie J. and Hampton, Matthew (2017) Timing recovery after the cretaceous/paleogene boundary: evidence from Brazos River, Texas. Journal of Foraminiferal Research, 47 (3). pp. 229-238. ISSN 0096-1191

Access from the University of Nottingham repository:

http://eprints.nottingham.ac.uk/44406/1/Leighton-Hart%20etal-Pearl_version.pdf

4   TIMING RECOVERY AFTER THE CRETACEOUS/PALEOGENE BOUNDARY:

5   EVIDENCE FROM BRAZOS RIVER, TEXAS

6

7   ANDREW D. LEIGHTON[1], MALCOLM B. HART[1,4], CHRISTOPHER W. SMART[1],

8   MELANIE J. LENG[2] AND MATTHEW HAMPTON[3]

9

10   [1]School of Geography, Earth and Environmental Sciences, Plymouth University, Plymouth, PL4

11   8AA, UK

12   [2]NERC Isotope Geosciences Facilities, British Geological Survey, Nottingham NG12 5GG, UK

13   & School of Geography, University of Nottingham, University Park, Nottingham NG7 2RD, UK

14   [3]Network Stratigraphic Consulting Ltd, Harvest House, Cranborne Road, Potters Bar,

15   Hertfordshire EN6 3JF, UK

16   [4]Correspondence author E-mail: mhart@plymouth.ac.uk

17

18

19

20   ABSTRACT

21

22   As part of an on-going re-assessment of the Cretaceous/Paleogene boundary in the

23 Brazos River area, Falls County, Texas, a number of new exposures have been described. One of

24 these, at Riverbank South, provides a near-continuous record of the lowermost Paleocene. It is

25 from this succession that stable isotope analysis of bulk organic matter (δ^{13}C and C/N) and

26 mono-specific samples of the benthic foraminifera *Lenticulina rotulata* Lamarck (δ^{18}O and δ^{13}C)

27 yields an orbitally-tuned stable isotope record, which allows the timing of events adjacent to the

28 Cretaceous/Paleogene boundary to be determined. Using this cyclicity, it is suggested that the

29 on-set of biotic recovery began ~40,000 years after the impact (near the base of Zone Pα) and

30 that more significant recovery of planktic foraminifera and calcareous nannofossils began close

31 to the base of Zone P1a, some 85,000–100,000 years post-impact. The data also appear to record

32 the presence of the earliest Paleocene DAN-C2 and Lower C29n hyperthermal events and that

33 these events appear to be an accentuated segment of this orbital cyclicity.

34

36   INTRODUCTION

37

38   The Cretaceous/Paleogene (K/Pg) mass extinction event is not the most severe of the

39   major extinction events in Earth's history but it is one of the most studied (Twitchett, 2006).

40   There were synchronous extinctions (Keller et al., 2009) in both the marine and terrestrial realms

41   including some invertebrates (e.g., ammonites), calcareous nannofossils, planktic foraminifera

42   and non-avian dinosaurs. A bolide impact at Chicxulub in the Yucatan Peninsula, Mexico, is

43   now generally accepted as a major cause of the extinction event (MacLeod et al., 2007), despite

44   on-going discussions (Schulte et al., 2010) regarding the timing of the extinctions and the

45   changes to global climate caused by the eruption of the Deccan volcanic centre in India (Adatte

46   et al., 2014; Keller, 2014; Punekar et al., 2014).

47   The K/Pg boundary on the Brazos River and its tributaries in Falls County, Texas (Fig. 1)

48   has been extensively studied (Hansen et al., 1987; Yancey, 1996; Keller et al., 2009; Adatte et

49   al., 2011; Hart et al., 2011, 2012) although there are on-going debates over the placement of the

50   boundary event in that area. Many of the discussions relate to the nature of the boundary

51   complex exposed in the Brazos River area, which has been interpreted as either tsunami deposits

52   associated with the Chicxulub impact (Bourgeois et al., 1988; Keller et al., 2003, 2009), a series

53   of storm deposits (Gale, 2006) or a succession of storm deposits resting on a tsunami-generated

54   erosion surface (Yancey, 1996; Hart et al., 2012; Yancey & Liu, 2013). At its base, the boundary

55   complex contains re-worked, impact-derived spherules, overlain by discrete sandstone bodies

56   (Hart et al., 2012) with hummocky cross-stratification, climbing ripples, complex bioturbation

57   and fossil-rich siltstone inter-beds. To date, investigations of this boundary have focused mainly

58   on exposures in the bed of the Brazos River close to the Rt. 413 bridge, the creeks (Darting

59   Minnow and Cottonmouth) or cored material. Recently, a new section on the Brazos riverbank,

60   which crops out between Cottonmouth and Darting Minnow creeks (8.5 km south of the Rt. 413

61   bridge), has been re-discovered and described (Plummer, 1926; Hart et al., 2012, figs. 2–4). This

62   exposure, known as River Bank South (RBS), is laterally continuous along a >100 m long cliff

63   and is currently the most complete exposure of the K/Pg boundary in the area at the present time

64   (Fig. 2). There have, however, been times between 1926 and 2011 when the outcrop was covered

65   by river-derived sediments.

66   The RBS succession exposes the uppermost part of the Corsicana Mudstone Formation

67   (uppermost Maastrichtian). The volcanic ash seen in Cottonmouth Creek, 45 cm below the base

68   of the 'Event Bed' (Keller et al.,2007; Hart et al., 2012) has not been recorded despite quite

69   extensive clearance of the outcrop. This volcanic ash, fully documented by Hart et al. (2012, p.

70   75–77) has been recorded within the Corsicana Mudstone Formation just north of the Rt. 413

71   bridge at a location described as River Bank North (RBN on Fig. 1). The thickness of the

72   Corsicana Mudstones between the volcanic ash and the tsunami-generated erosion surface is

73   variable, as would be expected below such an erosive surface. The conglomerate of re-deposited

74   calcareous mudstone nodules that marks the base of the 'Event Bed' succession in the bed of the

75   Brazos River immediately downstream of the Rt. 413 bridge is also indicative of the levels of

76   down-cutting by the tsunami. In Darting Minnow Creek the 'Event Bed' is present in the

77   waterfall succession but, traced downstream, the Maastrichtian mudstones are directly overlain

78   by Paleocene strata with the level of the 'Event Bed' represented by only an erosion surface. The

79   absence of the 'Event Bed' was also recorded in the nearby Mullinax 3 core (Adatte et al., 2011;

80   Hart et al., 2012). This level of field investigation and understanding is required prior to the

4

81 careful collection of representative suites of samples from the various localities and the

82 subsequent micropaleontological investigations.

83

84   METHODOLOGY

85

86   Planktic foraminifera have been extensively studied (Keller, 1989; Keller et al., 2009;

87 Abramovich et al., 2011) in this area and they clearly demonstrate the typical K/Pg mass

88 extinction pattern. Fewer investigations of benthic foraminifera have been undertaken (Plummer,

89 1926, 1931; Cushman, 1946; Hart et al., 2011; Leighton, 2014), even though they are highly

90 diverse and abundant throughout the K/Pg boundary succession. Figure 3 shows the

91 lithostratigraphy, nature of the sediments and some of the more important benthic foraminifera.

92 This assemblage is typical of the Gulf Coastal Plain area (Plummer, 1926, 1931; Cushman, 1946;

93 Olsson et al., 1996; Culver, 2003; Schulte & Speijer, 2009). As indicated by Hart et al. (2011,

94 2012), both the latest Maastrichtian and earliest Paleocene assemblages are typical of an inner to

95 mid-shelf setting with a water depth of 50–100 m based on the analysis of morphotypes (see

96 Koutsoukos & Hart, 1990). This so-called 'Midway-type assemblage' (Berggren & Aubert,

97 1975) is in contrast to the deeper-water 'Velasco-type assemblage' (Schnitker, 1979) that has

98 been described from northeast Mexico (Alegret & Thomas, 2001 and references therein).

99   Here we report stable isotope ratios obtained from the benthic species *Lenticulina*

100 *rotulata* Lamarck, an epifaunal/semi-infaunal taxon (Koutsoukos & Hart, 1990) that is abundant

101 throughout the succession and has been used by other authors (Keller et al., 2009; Adatte et al.,

102 2011) for stable isotope analysis at other K/Pg boundary locations. Specimens for the stable

103 isotope analysis were obtained by normal micropaleontological processing techniques. The bulk

5

104   sediment was air dried, weighed and then soaked in white spirit (Stoddart Spirit) for ~4 hours,

105   after which the excess white spirit was removed by filtering. Samples were then immersed in de-

106   ionised water for ~12 hours before washing through a 45 μm sieve, and then dried in an oven at

107   20°C. Once dry, the >45 μm residues were dry sieved into the >500 μm, 500–250 μm, 250–150

108   μm and 150–45 μm size fractions. If the samples were not fully disaggregated the whole process

109   was repeated 2 or even 3 times. All samples were processed in stratigraphical order.

110   Individual specimens of *L. rotulata* from three different size fractions were analysed to

111   assess the isotopic variations with specimen size (= growth or ontogeny). Specimens from the

112   >500 μm, 500–250 μm and 250–150 μm size fractions were checked by both optical and electron

113   microscopy for evidence of re-crystallization or chamber infilling. Clean specimens were

114   weighed, as approximately 15–100 mg were required for the isotope analysis. For the >500 μm

115   size fraction, this equated to 2–3 individuals, while 4–6 and 9–14 individuals were needed from

116   the 500–250 μm, and 250–150 μm fractions respectively. Measurements of $\Delta^{13}C$ and $\delta^{18}O$ were

117   performed on a GV IsoPrime mass spectrometer plus Multiprep device, located in the National

118   Isotope Geosciences Laboratory (NIGL), Keyworth, Nottingham. Isotope values ($\delta^{13}C$, $\delta^{18}O$) are

119   reported as per mille (‰) deviations of the isotopic ratios ($^{13}C/^{12}C$, $^{18}O/^{16}O$) calculated to the

120   VPDB scale using a within-run laboratory standard calibrated against NBS standards. Analytical

121   reproducibility of the standard calcite (KCM) is < 0.1‰ for $\delta^{13}C$ and $\delta^{18}O$.

122   After an acid wash to remove any carbonate material, $\delta^{13}C$ and C/N were measured on

123   the organic material by combustion in a Costech Elemental Analyser (EA) on-line to a VG Triple

124   Trap and Optima dual-inlet mass spectrometer (also located at NIGL). Values of $\delta^{13}C$ were

125   calculated to the VPDB scale using a within-run laboratory standards calibrated against NBS18,

126   NBS-19 and NBS22. Replicate analysis of well-mixed samples indicated a precision of + <0.1‰

127   (1 SD). Ratios of C/N were calibrated against an Acetanilide standard. Replicate analysis of

128   well-mixed samples indicated a precision of + <0.1.

129

130   RESULTS

131

132   The stable isotope data from *L. rotulata* are shown in Figure 4. As there is a significant

133   degree of reworking in the lowermost Paleocene, it is possible that the first 50 cm of the

134   Paleocene *may* include a re-worked signal from the Maastrichtian, *despite* the excellent

135   preservation. It is evident that the large δ^{13}C negative excursion that is often recorded

136   immediately above the K/Pg boundary (Fig. 5) is not present in the RBS section (see Martinez-

137   Ruiz et al., 1994; Hart et al., 2005, fig. 10; Lamolda et al., 2016, fig. 7; Hart et al., 2016, fig. 4).

138   This is unsurprising as the global, post-impact iridium anomaly is also absent from this

139   succession (Gertsch & Keller, 2012).

140   There is a full discussion of the K/Pg boundary at River Bank South given by Hart et al.

141   (2012). Following the agreed definition of the Global Stratotype Section and Point (GSSP)

142   provided by Molina et al. (2006), the boundary is the erosion surface generated by the tsunami

143   that resulted from the Chicxulub impact, with the overlying spherule bed and storm-derived

144   sandstones and siltstones representing the lowermost Paleocene. In more distal areas (from the

145   impact) such as Stevns Klint (Denmark), the Bottacione Gorge and Contessa Highway

146   successions near Gubbio (Italy), Gams (Austria), El Kef (Tunisia), Agost (Spain) and Caravaca

147   (Spain) the boundary hiatus is immediately overlain by sediments containing the iridium

148   anomaly and the negative δ^{13}C isotope excursion (see, for example, Lamolda et al., 2016, fig. 7),

149   neither of which are recorded in the Brazos River successions.

150   In the RBS succession, a series of gradually increasing, cyclical (?), stable isotope

151   excursions are recorded up-section into the Paleocene (Fig. 4). The >500 μm signal records these

152   excursions well, but the amplitude of each excursion increases as the size and, therefore,

153   maturity, of the *L. rotulata* specimens decreases. This indicates that the size (= age) of the

154   benthic foraminifera test is inversely proportional to the $\delta^{18}O$ and $\delta^{13}C$ signals. The amplitude of

155   the cyclicity in these excursions increases from the K/Pg boundary to within Zone P1a, where the

156   largest excursions (~6‰ and >5‰ in $\delta^{18}O$ and $\delta^{13}C$ respectively) in the smallest size fraction are

157   recorded. The excursions occur in all of the size fractions in the same interval, indicating that the

158   isotope signal appears to be genuine.

159   Cross-plots of $\delta^{18}O$ and $\delta^{13}C$ are often used extensively in paleoceanography (e.g.,

160   Wendler et al., 2013) to identify both benthic and planktic foraminifera niches (e.g., Birch et al.,

161   2013 and references therein). In our case, only data from a single benthic taxon is used and any

162   scatter, therefore, shows only the variability of the stable isotope signal with the size of

163   specimens analysed (= growth).

164   The bulk organic $\delta^{13}C_{org}$ is similar to the benthic foraminiferal $\delta^{13}C_{carbonate}$ especially

165   around the major excursions in Zone P1a (Fig. 5). Bulk $\delta^{13}C_{org}$ shows a negative excursion of

166   >1‰, followed by a positive excursion of >1‰. Bulk $\delta^{13}C_{org}$ shows a cyclical pattern of positive

167   and negative excursions, the magnitude of which increases up-section, similar to benthic

168   foraminiferal $\delta^{13}C_{carbonate}$. The carbon/nitrogen (C/N) ratio increases to >10 in this interval which

169   would normally be interpreted as a greater contribution of terrestrial organic material (Fig. 5; see

170   Sampei & Matsumoto, 2001 and Lamb et al.,2007).

171   There is a variable response in the foraminifera >500 μm, 500–250 μm and 250–150 μm

172   size fraction $\delta^{18}O$ data, with the greatest variation within the smallest (usually the more juvenile)

173   specimens. This ontogenetic variation in stable isotope data in benthic foraminifera has been

174   reported before using extant material (Schumacher et al., 2010) from the Indian Ocean, where

175   the variation was attributed to the infaunal mode of life, with juveniles residing at a greater depth

176   in the sediment than the larger adults. Ishimura et al. (2012) have confirmed this variation,

177   although they used the weight (i.e., calcification) of the specimens rather than overall

178   dimensions. In their study of living foraminifera, the lightest and, therefore, the youngest and –

179   though not discussed – the smallest forms recorded the largest negative excursions. Wendler et

180   al. (2013), reported a large variation in *Lenticulina* spp. stable isotope data from the Turonian

181   (Wendler et al., 2013, fig. 6) and this was attributed to the opportunistic life-style of the genus

182   (*op. cit*., p. 22). These authors suggest that, for most of the benthic taxa used in their analysis,

183   between 1 and 22 specimens were required in order to perform the stable isotope analysis. If

184   *Lenticulina* spp. are recording significant stable isotope variability with size (both ontogenetic

185   change and changes in life position *vis á vis* the sediment surface) then this might explain the

186   variability recorded by Wendler et al. (2013, p. 6). As many other authors (Keller et al., 2007,

187   2009) have used this genus from a range of size fractions their data may have been compromised

188   by this ontogenetic variability. This relationship has previously been described from planktic

189   foraminifera (Bornemann & Norris, 2007; Birch et al., 2013), where individuals are known to

190   change their position in the water column during ontogeny, but has rarely been reported in

191   studies of benthic foraminifera.

192   Whilst there is a close agreement between the results of all three size fractions, it is the

193   250–150 μm size fraction (juveniles) that displays the greatest variability in the $\delta^{18}O$ data (Fig.

194   4). These results indicate that there is a clear variation in $\delta^{18}O$ and $\delta^{13}C$ with size and that

195   comparisons with data generated from 'bulk' or randomly selected individuals may be invalid.

196   The graphs in Figure 4 show that only a profile based on standardised samples can be used in a

197   reliable way to determine events. The key features of the stable isotope data are presented below.

198   The lowermost Paleocene 'large' negative $\delta^{13}C$ excursion (Hart et al., 2005, fig. 10;

199   Schulte et al., 2010; Hart et al., 2016, fig. 4; Lamolda et al., 2016, fig. 7) is not evident (except

200   perhaps in the fine fraction data: Fig. 5). This is because the reworked spherule-rich bed and the

201   sandstones of the 'Event Bed' represent a disturbed environment in which the stable isotope

202   signal has been lost by erosion or completely masked by sediment mixing. The pattern of $\delta^{18}O$

203   and $\delta^{13}C$ excursions above the 'Event Bed' appears cyclical and probably represents an orbital

204   forcing. A record of orbital cyclicity is well-known in the Maastrichtian (Hart et al., 2005, fig. 9;

205   Batenberg et al., 2012, 2014) and Paleocene (Zachos et al., 2010; Westerhold et al., 2012) and

206   the cyclicity observed in our RBS succession is almost certainly that of the 21kyr precession

207   signal. Although no obvious sedimentary cycles are observed in the lowermost Paleocene

208   deposits of Texas (Fig. 2), there are distinctive carbonate-mudstone cycles recorded in the coeval

209   Lower Paleocene sediments of the Braggs, Mussel Creek (Hart et al., 2013, fig. 7), Miller's Ferry

210   (Olsson et al., 1996) and Moscow Landing (Hart et al., 2013, fig. 12) successions in Alabama.

211

212   TIMING OF EVENTS

213

214   In the chalks of the Sigerslev Member (Surlyk et al., 2006) exposed in the Stevns Klint

215   succession, the stable isotope data (Hart et al., 2005, fig. 10) appear to record a precessional

216   cyclicity, which was also recorded in the Maastricht chalk succession of the Netherlands

217   (Schiøler et al., 1997) and in the Maastrichtian successions on the north coast of Spain

218   (Batenberg et al., 2012, 2014). The 'Grey Chalk' (= Højerup Member) of the Stevns Klint

219 succession, which displays visible signs of sediment transport and the formation of 'mounds' on

220 the Maastrichtian sea floor, records no cyclicity as a result of sediment mixing. The overlying

221 Fish Clay (= Fiskeler Member), however, records (Hart et al., 2016, fig. 4) the characteristic,

222 negative $\delta^{13}C$ excursion (see Molina et al., 2006) and a number of other $\delta^{13}C$ excursions that

223 diminish in magnitude up-section (see Martinez-Ruiz et al., 1994). The total thickness of the Fish

224 Clay may, if these are precessional cycles, represent 40,000 – 60,000 years. This interval of time

225 is represented by only <50 cm of sediment (after compaction), implying a remarkably slow rate

226 of sedimentation. This is, however, to be expected as – in the chalk sea of northwest Europe – a

227 loss of calcareous nannofossils and planktic foraminifera would significantly reduce the

228 sediment supply. The background supply of siliciclastic sediment (largely clays) normally

229 represents <1% of uppermost Cretaceous chalks in north-west Europe (Hancock, 1976) and the

230 loss of carbonate sediment supply following the K/Pg mass extinction event explains the reduced

231 sedimentation rate. The Fish Clay contains a diverse and abundant assemblage of

232 dinoflagellatecysts (Hansen, 1977; Hultberg, 1985, 1986, 1987; Hultberg & Malmgren, 1987),

233 but this abundance must also be viewed in the context of the reduced sedimentation rate.

234   In Texas, however, the dominant sediment supply is siliciclastic and the stable isotope

235 data (Fig. 4) do not show the same levels of condensation, despite a similar loss of calcareous

236 nannofossils and planktic foraminifera at the level of the K/Pg extinction event. The large $\delta^{13}C$

237 negative excursion is missing and there are, therefore, ~2 excursions prior to the P0/Pα

238 boundary. This indicates ~40,000 years of elapsed time between the extinction event and the

239 onset of 'recovery'. Berggren & Pearson (2005) have also indicated ~30,000 years for the

240 duration of Zone P0. As there are a further 2–3 cycles to the Pα/P1a boundary (Fig. 4), this

241 places the on-set of a more comprehensive recovery of the plankton at ~80,000–100,000 years.

242   At the level of the Middle Sandstone Bed (MSB) and the Dirty Sandstone Bed (DSB) the

243   benthic foraminifera are at their most diverse (Fig. 3) with large specimens recorded. Many of

244   these nodosariids are exceptionally long and, as the apical spine and the aperture are often

245   present, unlikely to have suffered any disturbance or transport. The presence of these large

246   specimens was noted by Plummer (1926) as being a particular characteristic of the RBS section.

247   Following the models of Emery & Myers (1996, fig. 6.14) and Oxford et al. (2000, 2004), this

248   would suggest that the MSB/DSB interval represents a zone of maximum flooding, which may

249   contribute to the increased $\delta^{13}C$ peak. There is also a peak in the $\delta^{13}C_{organic}$ record (Fig. 5), which

250   may indicate a greater supply of terrestrial organic material and increased surface run-off from

251   the land.

252

253   PALEOCENE HYPERTHERMAL EVENTS

254

255   The Paleocene world was characterised by a continuing greenhouse condition and, within

256   it, there are a number of significant – but transient – hyperthermal events (Bralower et al., 2002;

257   Speijer, 2003; Petrizzo, 2005; Bernaola et al., 2007; Quillévéré et al., 2008; Bornemann et al.,

258   2009; Coccioni et al., 2010). Whilst the most prominent is the Paleocene–Eocene Thermal

259   Maximum or PETM (Zachos et al., 2001, 2010), earlier events are also quite significant and, in

260   carbonate-rich sediments, are associated with a drop in carbonate production and/or enhanced

261   dissolution. The DAN-C2 and Lower C29n events (Coccioni et al., 2010) have been identified in

262   the Contessa Highway section (Gubbio, Italy) and a small number of ODP/DSDP sites

263   (Quillévéré et al., 2008). None of these locations are in a shallow-water, mid-shelf environment,

264   comparable with the Brazos River area. In the RBS succession the maximum $\delta^{13}C$ excursion

12

265   appears to be coeval with the Lower C29n event while the Dan-C2 event (represented by the

266   upper Pα and lower P1a zones) is less pronounced.

267   The significant negative $\delta^{18}O$ and $\delta^{13}C$ excursion near the NP1/NP2 boundary

268   approximately 2.5 m above the K/Pg boundary represents a possible <6°C warming that is

269   relatively short-lived. This appears to be coeval with the Lower C29n hyperthermal event

270   (Coccioni et al., 2010) while a smaller, but still significant, negative $\delta^{18}O$ and $\delta^{13}C$ excursion

271   below this near the Pα/P1a boundary appears to be coeval with the DAN-C2 hyperthermal event.

272   The DAN-C2 hyperthermal event (Quillévéré et al., 2008; Coccioni et al., 2010) occurs within

273   the lower P1a and NP1 biozones, while the Lower C29n hyperthermal event occurs within the

274   uppermost part of the NP1 calcareous nannofossil biozone and within the P1a planktic

275   foraminiferal biozone. The hyperthermal events at Contessa Highway (Coccioni et al., 2010)

276   appear coeval with the timing of the excursions in the RBS section as the biostratigraphy is well-

277   constrained. The biostratigraphy within the RBS section is reliable and accurate, with the

278   calcareous nannofossil data based on the same samples as those used in the analysis of the

279   benthic and planktic foraminifera and the stable isotope analyses. The distribution of the planktic

280   foraminifera in the RBS succession is exactly comparable to that recorded in the Brazos-1

281   section by Liu (pers. comm., 2012, 2013) and the Brazos River outcrop immediately south of the

282   Rt. 413 bridge. The distribution of taxa is also in agreement with that recorded in the Mullinax-1

283   borehole (Abramovich et al., 2011; Keller & Adatte, 2011 and papers cited therein), though our

284   placing of the K/Pg boundary is different to that recorded by these authors. The calcareous

285   nannofossil data allow the placing of NP1 and NP2, with direct comparisons to the successions

286   in Agost (Lamolda et al., 2016), Caravaca (Lamolda et al., 2005), El Kef (Pospichal, 1994) and

287   Elles (Gardin, 2002). The magnitude of the stable isotopic excursions recorded in the Brazos

288 River area are larger than those observed near Gubbio (Coccioni et al., 2010), although this can

289 be attributed to the use of species-specific benthic foraminifera within this study rather than bulk

290 rock samples.

291   The $\delta^{13}C_{organic}$ isotope data (Fig. 5) are in close agreement with the species-specific

292 foraminiferal isotope data, with the $\delta^{13}C_{organic}$ signal closely reflecting the excursions of the

293 species-specific $\delta^{13}C_{carbonate}$ isotope data. This indicates that the carbon source for both the

294 foraminifera and the sediments ($\delta^{13}C_{organic}$ and $\delta^{13}C_{carbonate}$) is the same. An increase in the C/N

295 ratio >10 indicates a more terrestrial origin for organic material (Fig. 5). The marked increase in

296 the C/N ratio coincides with the marked negative $\delta^{13}C$ excursion of the foraminiferal isotopic

297 data and suggests that there was a greater supply of terrestrial plant material and increased

298 surface run-off from the land onto the shelf. This mechanism could also account for the

299 fluctuations of the $\delta^{18}O$ isotope signal as this could be marking an increase of freshwater into the

300 system and, therefore, much lighter isotopic values. Increased surface run-off from the land, as a

301 result of hydrological changes, is a particular feature that often characterizes hyperthermal events

302 (see Manners et al., 2013, and references therein), so the interpretation of increased freshwater

303 input into the Brazos River area supports this conclusion.

304   The general warming recorded by the DAN-C2 and Lower C29n events (Coccioni et al.,

305 2010) appears to be associated with the interval of time close to the last of the eruption phases of

306 the Deccan Plateau (Chenet et al., 2007, 2009), although there is an on-going re-evaluation of the

307 ages of the Deccan volcanics (e.g., Schoene et al., 2015). The timing of the hyperthermal

308 event(s) in the Brazos River area suggests that the DAN-C2 and Lower C29n event may be more

309 widespread than previously suggested. The stable isotope data from the Brazos River area may

310 be astronomically tuned, a feature of the DAN-C2 event (Quillévéré et al., 2008). An

14

311   astronomical signal has also been suggested (Jolley et al., 2011; Gilmour et al., 2012, 2013,

312   2014) following an analysis of the sediments within the Boltysh impact crater in Ukraine. There

313   are four climate-induced cycles (Gilmour et al., 2013, 2014) between the K/Pg boundary and

314   what has been identified as the DAN-C2 event. If this cyclicity, and the DAN-C2 event (and

315   Lower C29n event), are confirmed from terrestrial, shallow marine (Brazos River area) and

316   deeper marine successions, then these events are comparable to other Paleogene hyperthermal

317   events that are recorded globally and from a wide range of environments (both terrestrial and

318   marine).

319

320   CONCLUSIONS

321

322   Stable isotope data derived from size-controlled samples of *Lenticulina rotulata* Lamarck

323   across the K/Pg boundary in the Brazos River area, Texas, indicate that early recovery began

324   ~40,000 years post-impact and that a more significant recovery was under-way by 80,000–

325   100,000 years post-impact. The data also suggest that the DAN-C2 and Lower C29n

326   hyperthermal events have been detected in the mid-shelf environment represented by the

327   sediments of the Kincaid Formation, Brazos River area, Falls County, Texas. These events

328   appear to be coeval with those identified from the Contessa Highway K/Pg section in Italy, and

329   occur at the same stratigraphic level as determined by both calcareous nannofossil and planktic

330   foraminferal biozonation schemes. The variation in δ^{18}O and δ^{13}C recorded in the various size

331   fractions of the mono-specific samples used in our investigation raises issues for stable isotope

332   data derived from variously-sized foraminifera or samples of mixed benthic assemblages. The

333   data do, however, indicate that fossil material is showing stable isotope variations in line with

334 those recorded in modern (living) foraminifera. The stable isotopic signal from the Brazos River

335 area indicates an increased amount of surface run-off (freshwater input) in the early Paleocene.

336 The increased surface run-off, hyperthermal events and bulk organic $\delta^{13}C$ geochemical signals

337 indicate that the earliest Paleocene immediately after the K/Pg boundary event was a period of

338 climatic instability and fluctuating environmental parameters.

339

340

341

342

352

353 REFERENCES

354

355 Abramovich, S., Keller, G., Berner, Z., Cymbalista, M., and Rak, C., 2011, Maastrichtian

356   planktic foraminiferal biostratigraphy and paleoenvironment of Brazos River, Falls

357   County, Texas, USA, *in* Keller, G., and Adatte, T., (eds.), The end-Cretaceous mass

358   extinction and the Chicxulub impact in Texas: SEPM Special Publication, v. 100, p. 123–

359   156.

360 Adatte, T., Keller, G., and Baum, G. R., 2011, Age and origin of the Chicxulub impact and

361   sandstone complex, Brazos River, Texas: Evidence from lithostratigraphy and

362   sedimentology, *in* Keller, G., and Adatte, T. (eds.), The end-Cretaceous mass extinction

363   and the Chicxulub impact in Texas: SEPM Special Publication, v. 100, p. 43–80.

364 Adatte, T., Fantasia, A., Samant, B., Mohabey, D., Font, E. Keller, G., Khozyem, H., and

365   Gertsch, B., 2014, Deccan volcanism: a main trigger of environmental changes leading to

366   the K/Pg mass extinction?: Communicações Geológicas, v. 101, Especial lll, p. 1435–

367   1437.

368 Alegret, L., and Thomas, E., 2001, Upper Cretaceous and lower Paleogene benthic foraminifera

369   from northeastern Mexico: Micropaleontology, v. 47, p. 269–316.

370 Batenberg, S. J., Sprovieri, M., Gale, A. S., Hilgen, F. J., Hüsing, S., Laskar, J., Liebrand, D.,

371   Lirer, F., Orue-Extebarria, X., Pelosi, N., and Smit, J., 2012, Cyclostratigraphy and

372   astronomical tuning of the Late Maastrichtian at Zumaia (Basque country, Northern

373   Spain): Earth and Planetary Science Letters, v. 359–360, p. 264–278.

374 Batenberg, S. J., Gale, A. S., Sprovieri, M., Hilgen, F. J., Thibault, N., Boussaha, M., Orue-

375   Etxebarria, X., 2014, An astronomical time scale for the Maastrichtian based on the

376   Zumaia and Sopelana sections (Basque country, northern Spain): Journal of the

377   Geological Society, London, v. 171, p. 165–180.

378   Berggren, W. A., and Aubert, J., 1975, Paleocene benthonic foraminiferal biostratigraphy,

379   paleobiogeography and paleoecology of Atlantic-Tethyan regions: Midway-type fauna:

380   Palaeogeography, Palaeoclimatology, Palaeoecology, v. 18, p. 73–192.

381   Berggren, W. A., and Pearson, P. N., 2005, A revised tropical to subtropical Paleogene

382   planktonic foraminiferal zonation: Journal of Foraminiferal Research, v. 35, p. 279–298.

383   Bernaola, G., Baceta, J. I., Orue-Extebarria, X., Alegret, L., Martin-Rubio, M., Arostegui, J., and

384   Dinarès-Turell, J., 2007, Evidence of an abrupt environmental disruption during the mid-

385   Paleocene biotic event (Zumaia section, western Pyrenees): Geological Society of

386   America Bulletin, v. 119, p. 785–795.

387   Birch, H., Coxall, H. K., Pearson, P. N., Kroon, D., O'Regan, M., 2013, Planktonic foraminifera

388   stable isotopes and water column structure: Disentangling ecological signals: Marine

389   Micropaleontology, v. 101, p. 127–145.

390   Bornemann, A., and Norris, R. D., 2007, Size-related stable isotope changes in Late Cretaceous

391   planktic foraminifera: Implications for paleoecology and photosymbiosis: Marine

392   Micropaleontology, v. 29, p. 32–42.

393   Bornemann, A., Schulte, P., Sprong, J., Steurbaut, E., Youssef, M., and Speijer, R. P., 2009,

394   Latest Danian carbon isotope anomaly and associated environmental change in the

395   Southern Tethys (Nile basin, Egypt): Journal of the Geological Society, London, v. 166,

396   p. 135–142.

397   Bourgeois, J., Hansen, T. A., Wiberg, P. L., and Kauffman, E. G., 1988, A tsunami deposit at the

398   Cretaceous-Tertiary boundary in Texas: Science, v. 241, p. 567–570.

399   Bralower, T. J., Premoli Silva, I., and Malone, M. J., 2002, New evidence for abrupt climate

400   change in the Cretaceous and Paleogene: an Ocean Drilling Program expedition to

401   Shatsky Rise, northwest Pacific: GSA Today, v. 12, p. 4–10.

402   Chenet, A. L., Quidelleur, X., Fluteau, F., Courtillot, V., and Bajpai, S., 2007, ^{40}K–^{40}Ar dating of

403   the Main Deccan large igneous province: Further evidence of KTB age and short

404   duration: Earth and Planetary Science Letters, v. 263, p. 1–15.

405   Chenet, A. L., Courtillot, V., Fluteau, F., Gerard, M., Quidelleur, X., Khadri, S. F. R., Subbaro,

406   K. V., and Thordarson, T., 2009, Determination of rapid Deccan eruptions across the

407   Cretaceous-Tertiary boundary using paleomagnetic secular variation: 2. Constraints from

408   analysis of eight new sections and synthesis for a 3500 m-thick composite section:

409   Journal of Geophysical Research, v. 114, B06103, DOI:10.1029/2008JB005644

410   Coccioni, R., Frontalini, F., Bancalà, G., Fornaciari, E., Jovane, L., and Sprovieri, M., 2010, The

411   Dan-C2 hyperthermal event at Gubbio (Italy): Global implications, environmental

412   effects, and cause(s): Earth and Planetary Science Letters, v. 297, p. 298–305.

413   Culver, S. J.,2003, Benthic foraminifera across the Cretaceous–Tertiary (K–T) boundary: A

414   review: Marine Micropaleontology, v. 47, p. 177–226.

415   Cushman, J. A., 1946, Upper Cretaceous foraminifera of the Gulf Coastal region of the United

416   States and adjacent areas: United States Geological Survey, Professional Paper, no. 206,

417   241 p.

418   Emery, D., and Myers, K. J, 1996, Sequence Stratigraphy: Blackwell Science, Oxford,297 p.

419   Gale, A. S., 2006, The Cretaceous-Palaeogene boundary on the Brazos River, Falls County,

420   Texas: Is there evidence for impact-induced tsunami sedimentation?: Proceedings of the

421   Geologists' Association, London, v. 117, p. 173–185.

422   Gardin, S., 2002, Late Maastrichtian to early Danian calcareous nannofossils at Elles (Northwest

423   Tunisia). A tale of one million years across the K-T boundary: Palaeogeography,

424   Palaeoclimatology, Palaeoecology, v. 178, p. 211–231.

425   Gertsch, B., and Keller, G., 2012, Platinum group element (PGE) geochemistry of Brazos

426   sections, Texas, USA, *in* Keller, G., and Adatte, T. (eds.), The end-Cretaceous mass

427   extinction and the Chicxulub impact in Texas, SEPM Special Publication, v. 100, p. 227–

428   249.

429   Gilmour, I., Jolley, D. J. W., Daley, R. J., Kelley, S. P., and Gilmour, M. A., 2012, A complete

430   high resolution record of the Dan-C2 hyperthermal event in the lacustrine sediments of

431   the Boltysh Impact Crater. Geophysical Research Abstracts, v. 14, EGU2012-7870-2

432   [abstract].

433   Gilmour, I., Gilmour, M., Jolley, D., Kelly, S., Kemp, D., Daly, R., and Watson, J., 2013, A

434   high-resolution nonmarine record of an early Danian hypothermal event, Boltysh crater,

435   Ukraine: Geology, v. 41, p. 783–786.

436   Gilmour, I., Jolley, D., Kemp, D., Kelley, S., Gilmour, M., Daly, R., and Widdowson, M., 2014,

437   The early Danian hyperthermal event at Boltysh (Ukraine): Relation to Cretaceous-

438   Paleogene boundary events, *in* Keller, G., and Kerr, A. C. (eds.), Volcanism, Impacts,

439   and Mass Extinctions: Causes and Effects: Geological Society of America, Special Paper

440   No. 505, p. 133–146.

441   Hancock, J. M., 1976, The petrology of the chalk: Proceedings of the Geologists' Association,

442   London, v. 86, p. 499–535 [for 1975].

443   Hansen, J. M., 1977, Dinoflagellate stratigraphy and echinoid distribution in Upper

444   Maastrichtian and Danian deposits from Denmark: Bulletin of the Geological Society of

445   Denmark, v. 26, p. 1–26.

446   Hansen, T. A., Farrand, B. R., Montgomery, H. A., Billman, H. G., and Blechschmidt, G., 1987,

447   Sedimentology and extinction patterns across the Cretaceous-Tertiary boundary interval

448   in east Texas: Cretaceous Research, v. 8, p. 229–252.

449   Hart, M. B., Feist, S. E., Håkansson, E., Heinburg, C., Price, G. D., Smart, C. W., and

450   Watkinson, M. P., 2005, The Cretaceous-Palaeogene boundary succession at Stevns

451   Klint, Denmark: Foraminifers and stable isotope stratigraphy: Palaeogeography,

452   Palaeoclimatology, Palaeoecology, v. 224, p. 6–26.

453   Hart, M. B., Searle, S. R., Feist, S. E., Leighton, A. D., Price, G. D., Smart, S. W., and Twitchett,

454   R. J., 2011, The distribution of benthic foraminifera across the Cretaceous-Paleogene

455   boundary in Texas (Brazos River) and Denmark (Stevns Klint), *in* Keller, G., and Adatte,

456   T. (eds.), The end-Cretaceous mass extinction and the Chicxulub impact in Texas: SEPM

457   Special Publication, v. 100, p. 179–196.

458   Hart, M. B., Yancey, T. E., Leighton, A. D., Miller, B., Liu, C., Smart, C. W., and Twitchett, R.

459   J., 2012, The Cretaceous-Paleogene boundary on the Brazos River, Texas: new

460   stratigraphic sections and revised interpretations: Journal of the Gulf Coast Association

461   of Geological Societies, v. 1, p. 69–80.

462   Hart, M. B., Harries, P. J., and Cárdenas, A. L., 2013, The Cretaceous/Paleogene boundary

463   events in the Gulf Coast: Comparisons between Alabama and Texas: Gulf Coast

464   Association of Geological Societies, Transactions, v. 63, p. 235–255.

465 Hart, M. B., FitzPatrick, M. E. J., and Smart, C. W., 2016, The Cretaceous/Paleogene boundary:

466   Foraminifera, sea grasses, sea level change and sequence stratigraphy: Palaeogeography,

467   Palaeoclimatology, Palaeoecology, v. 441, p. 420–429.

468 Hultberg, S. U., 1985, Dinoflagellate studies of the Upper Maastrichtian and Danian in southern

469   Scandinavia: University of Stockholm, unpublished PhD Thesis, 189p.

470 Hultberg, S. U., 1986, Danian dinoflagellate zonation, the C-T boundary and the stratigraphical

471   position of the fish clay in southern Scandinavia: Journal of Micropalaeontology, v. 5, p.

472   37–47.

473 Hultberg, S. U., 1987, Palynological evidence for a diachronous low-salinity event in the C-T

474   boundary clay at Stevns Klint, Denmark: Journal of Micropalaeontology, v. 6, p. 35–40.

475 Hultberg, S. U., and Malmgren, B. A., 1987, Quantitative biostratigraphy based on Late

476   Maastrichtian dinoflagellates and planktonic foraminifera from Southern Scandinavia:

477   Cretaceous Research, v. 8, p. 211–228.

478 Ishimura, T., Tsunogai, U., Hasegawa, S., Nakagawa, F., Oi, T., Kitazato, H., Suga, H., and

479   Toyofuku, T., 2012, Variation is stable carbon and oxygen isotopes of individual benthic

480   foraminifera: Tracers for quantifying the magnitude of isotopic disequilibrium:

481   Biogeosciences, v. 9, p. 4353–4367.

482 Jolley, D., Gilmour, I., Gurov, E., Kelley, S., and Watson, J., 2011, Two large meteorite impacts

483   at the Cretaceous-Paleogene boundary: Geology, v. 38, p. 835–838.

484 Keller, G., 1989, Extended Cretaceous/Tertiary boundary extinctions and delayed population

485   change in planktonic foraminifera from Brazos River, Texas: Paleoceanography, v. 4, p.

486   287–332.

487 Keller, G., 2014, Deccan volcanism, the Chicxulub impact, and the end-Cretaceous mass

488 extinctions: Coincidences? Cause and effect? *in* Keller, G., and Kerr, A. C. (eds.),

489 Volcanism, Impacts, and Mass Extinctions: Causes and Effects: Geological Society of

490 America, Special Paper No. 505, p. 57–90.

491 Keller, G., Stinnesbeck, W., Adatte, T., and Stüben, D., 2003, Multiple impacts across the

492 Cretaceous-Tertiary boundary: Earth Science Reviews, v. 62, p. 327–363.

493 Keller, G., Adatte, T., Berner, Z., Harting, M., Baum, G., Prauss, M., Tantawy, A., and Stüben,

494 D., 2007, Chicxulub impact predates K–T boundary: New evidence from Brazos, Texas:

495 Earth and Planetary Science Letters, v. 255, p. 339–356.

496 Keller, G., Adatte, T., Berner, Z., Pardo, A., and Lopez-Oliva, L., 2009, Age and biotic effects of

497 the Chicxulub impact in Mexico: Journal of the Geological Society, London, v. 166, p.

498 393–411.

499 Koutsoukos, E. A. M., and Hart, M. B., 1990, Cretaceous foraminiferal morphogroup

500 distribution patterns, palaeocommunities and trophic structures: A case study from the

501 Sergipe Basin, Brazil: Transactions of the Royal Society, Edinburgh, Earth Sciences, v.

502 81, p. 221–246.

503 Lamb, A. L., Vane, C. H., Wilson, G. P., Rees, J. G., and Moss-Hayes, V. L., 2007, Assessing

504 δ^{13}C and C/N ratios from organic material in archived cores as Holocene sea level and

505 palaeoenvironmental indicators in the Humber Estuary, UK: Marine Geology, v. 244, p.

506 109–128.

507 Lamolda, M. A., Melinte, M. C., and Kaiho, K., 2005, Nannofloral extinction and survivorship

508 across the K-Pg boundary at Caravaca, southeastern Spain. Palaeogeography,

509 Palaeoclimatology, Palaeoecology, v. 224, p. 27–52.

510   Lamolda, M. A., Melinte-Dobrinescu, M. C., and Kaiho, K., 2016, Calcareous nannoplankton

511   assemblage changes linked to paleoenvironmental deterioration and recovery across the

512   Cretaceous-Paleogene boundary in the Betic Cordillera (Agost, Spain): Palaeogeography,

513   Palaeoclimatology, Palaeoecology, v. 441, p. 438–452.

514   Leighton, A. D., 2014, Benthic foraminiferal change and depositional history across the

515   Cretaceous–Paleogene (K/Pg) boundary in the Brazos River area, Texas: Plymouth

516   University Research Theses, unpublished PhD Thesis (available on the PEARL website).

517   MacLeod, K. G., Whitney, D. L., Huber, B. T., and Koeberl, C., 2007, Impact and extinction in

518   remarkably complete Cretaceous-Tertiary boundary sections from Demerara Rise,

519   tropical western North Atlantic: Geological Society of America Bulletin, v. 119, p. 101–

520   115.

521   Manners, H. R., Grimes, S. T., Sutton, P. A., Domingo, L., Leng, M. J., Twitchett, R. J., Hart, M.

522   B., Dunkley Jones, T., Pancost, R. D., Duller, R., and Lopez-Martinez, N., 2013,

523   Magnitude and profile of organic carbon isotope records from the Paleocene–Eocene

524   Thermal Maximum: Evidence from northern Spain: Earth and Planetary Science Letters,

525   v. 376, p. 220–230.

526   Martinez-Ruiz, F., Bernasconi, S., and McKenzie, J. A., 1994, Paleoceanographic changes across

527   the Cretaceous-Tertiary boundary: carbon and nitrogen isotope stratigraphy:

528   Mineralogical Magazine, v. 58, p. 561–562.

529   Molina, E., Alegret, L., Arenillas, I., Arz, J. A., Gallala, N., Hardenbol, J., Von Salis, K.,

530   Steurbaut, E., Vandenberghe, N., and Zaghbib-Turki, D., 2006, The global boundary

531   stratotype section and point for the base of the Danian Stage (Paleocene, Paleogene,

532   "Tertiary", (Cenozoic) at El Kef, Tunisia – original definition and revision: Episodes, v.

533   29, p., 263–278.

534 Olsson, R. K., Liu, C., and van Fossen, M., 1996, The Cretaceous-Tertiary catastrophic event at

535   Miller's Ferry, Alabama, *in* Ryder, G. et al. (eds.), The Cretaceous-Tertiary boundary

536   event and other catastrophes in earth history: Geological Society of America, Special

537   Paper 307, Boulder, Colorado, p. 263–277.

538 Oxford, M. J., Hart, M. B., and Watkinson, M. P., 2000, Micropalaeontological investigations of

539   the Oxford Clay: Geoscience in south-west England, v. 10, p. 9–13.

540 Oxford, M. J., Hart, M. B., and Watkinson, M. P., 2004, Foraminiferal characterization of mid-

541   Upper Jurassic sequences in the Wessex Basin (United Kingdom): Rivista Italiana di

542   Paleontologia e Stratigrafia, v. 110, p. 209–218.

543 Petrizzo, M. R., 2005, An early late Paleocene event on Shatsky Rise, northwest Pacific Ocean

544   (ODP Leg 198): Evidence for planktonic foraminiferal assemblage, *in* Bralower, T.J.,

545   Premoli Silva, I., & Malone, M.J. (Eds.), Proceedings of the Ocean Drilling Program,

546   Scientific Results, v. 198, p. 1–29.

547 Plummer, H. J., 1926, Foraminifera of the Midway Formation in Texas: University of Texas,

548   Bulletin, no. 2644, 201 p.

549 Plummer, H. J., 1931, Some Cretaceous foraminifera in Texas: University of Texas Bulletin, no.

550   3101, p. 109–203.

551 Pospichal, J. J., 1994, Calcareous nannofossils at the K-Pg boundary El Kef, Tunisia: no

552   evidence for stepwise, gradual or sequential extinctions: Geology, v. 22, p. 99–102.

553 Punekar, J., Mateo, P., and Keller, G., 2014, Effects of Deccan volcanism on paleoenvironment

554   and planktonic foraminifera: A global survey, *in* Keller, G., and Kerr, A. C. (eds.)

555   Volcanism, Impacts, and Mass Extinctions: Causes and Effects: Geological Society of

556   America, Special Paper No. 505, p. 91–116.

557   Quillévéré, F., Norris, R. D., Kroon, D., and Wilson, P. A., 2008, Transient ocean warming and

558   shifts in carbon reservoirs during the early Danian: Earth and Planetary Science Letters,

559   v. 265, p. 600–615.

560   Sampei, Y., and Matsumoto, E., 2001, C/N ratios in a sediment core from Nakaumi Lagoon,

561   southwest Japan – usefulness as an organic source indicator: Geochemical Journal, v. 35,

562   p. 189–205.

563   Schiøler, P., Brinkhuis, H., Roncaglia, L., and Wilson, G. J., 1997, Dinoflagellate biostratigraphy

564   and sequence stratigraphy of the type Maastrichtian (Upper Cretaceous), ENCI quarry,

565   The Netherlands: Marine Micropaleontology, v. 31, p. 65–95.

566   Schnitker, D., 1979,Cenozoic deep water benthic foraminifers, Bay of Biscay, *in* Montadert, L.

567   et al. (eds.), Initial Reports of the Deep Sea Drilling project, U.S. Government Printing

568   Office, Washington D.C., v. 48, p. 377–414.

569   Schoene, B., Samperton, K. M., Eddy, M. P., Keller, G., Adatte, T., Bowring, S. A., Khadri, S. F.

570   R., and Gertsch, B., 2015, U-Pb geochronology of the Deccan Traps and relation to the

571   end-Cretaceous mass extinction: Science, v. 347, p. 182–184.

572   Schulte, P., and Speijer, R., 2009, Late Maastrichtian-Early Paleocene sea level and climate

573   changes in the Antioch Church Core (Alabama, Gulf of Mexico margin, USA): a multi-

574   proxy approach: Geologica Acta, v. 7, 11–34.

575   Schulte, P., and 40 additional authors, 2010, The Chicxulub asteroid impact and mass extinction

576   at the Cretaceous-Paleogene boundary: Science, v. 327, p. 1214–1218.

577   Schumacher, S., Jorissen, F. J., Mackensen, A., Gooday, A. J., and Pays, O., 2010, Onogenetic

578   effects on stable carbon and oxygen isotopes in tests of live (Rose Bengal stained)

579   benthic foraminifera from the Pakistan continental margin: Marine Micropaleontology, v.

580   76, p. 92–103.

581   Speijer, R. P., 2003, Danian–Selandian sea-level change and biotic excursion on the southern

582   Tethyan margin (Egypt), *in* Wings, S. L. et al. (eds.), Causes and consequences of

583   globally warm climates in the Early Paleogene: Geological Society of America, Special

584   Paper, v. 369, p. 275–290.

585   Surlyk, F., Damholt, T., and Bjerager, M., 2006, Stevns Klint, Denmark: Uppermost

586   Maastrichtian chalk, Cretaceous–Tertiary boundary, and lower Danian bryozoans mound

587   complex: Bulletin of the Geological Society of Denmark, v. 54, p. 1–48.

588   Twitchett, R. J., 2006, The palaeoclimatology, palaeoecology and palaeoenvironmental analysis

589   of mass extinction events: Paleogeography, Palaeoclimatology, Palaeoecology, v. 232, p.

590   190–213.

591   Wendler, I., Huber, B. T., MacLeod, K. G., and Wendler, J. E., 2013, Stable oxygen and carbon

592   isotope systematic of exquisitely preserved Turonian foraminifera from Tanzania –

593   understanding isotopic signature in fossils: Marine Micropaleontology, v. 102, p. 1–33.

594   Westerhold, T., Röhl, U., and Laskar, J., 2012, Time scale controversy: Accurate orbital

595   calibration of the early Paleogene: Geochemistry, Geophysics, Geosystems, v. 13,

596   Q06015, DOI: 10.1029/2012GC004096

597   Yancey, T. E., 1996, Stratigraphy and depositional environments of the Cretaceous-Tertiary

598   boundary complex and basal Paleocene section, Brazos River, Texas: Transactions of the

599   Gulf Coast Association of Geological Societies, v. 46, p. 433–442.

600   Yancey, T. E., and Liu, C., 2013, Impact-induced sediment deposition on an offshore, mud

601   substrate continental shelf, Cretaceous-Paleogene boundary, Brazos River, Texas, USA:

602   Journal of Sedimentary Research, v. 83, p. 354–367.

603   Zachos, J. C., Pagani, M., Sloan, L., Thomas, E., and Billups, K., 2001, Trends, rhythms, and

604   aberrations in global climate 65 Ma to present: Science, v. 292, p. 686–693.

605   Zachos, J. C., McCarren, H., Murphy, B., Röhl, U., and Westerhold, T., 2010, Tempo and scale

606   of late Paleocene and early Eocene carbon isotope cycles: Implications for the origin of

607   hyperthermals: Earth and Planetary Science Letters, v. 299, p. 242–249.

608

611

612

613   FIGURE CAPTIONS

614

615   FIGURE 1. Locality map of the Brazos River area, Falls County, Texas (after Hart et al., 2012).

616

617   FIGURE 2. Sedimentary log of the K/Pg boundary succession exposed on the Brazos River at

618   RBS (based on Hart et al., 2012). The thin volcanic ash recorded in the uppermost Maastrichtian

619   of the Cottonmouth Creek succession (Hart et al., 2012) has not been recorded in the RBS

620   succession, despite digging into the Maastrichtian mudstones as far as river levels allowed.

621

622   FIGURE 3. Sedimentary log of the RBS succession, which also shows examples of a

623   representative selection of benthic foraminifera. The lithological symbols are explained in Figure

624   2 and the bed names follow Yancey (1996) including, from bottom to top, Hummocky Cross-

625   Stratification (HCS), Lower Calcareous Horizon (LCH), Middle Sandstone Bed (MSB), Dirty

626   Sandstone Bed (DSB), Upper Calcareous Horizon (UCH) and Rusty Pyrite Horizon (RPH).

627

628   FIGURE 4. Comparison of the $\delta^{18}O$ and $\delta^{13}C$ stable isotope data derived from an analysis of

629   *Lenticulina rotulata* Lamarck in the >500 μm, 500–250 μm and 250–150 μm size fractions. The

630   thinner black line marks the running average.

631

632   FIGURE 5. Bulk organic $\delta^{13}C$, fine fraction $\delta^{18}O/\delta^{13}C$ and C/N ratio data for the RBS succession.

633   The data are plotted against the same sedimentary log as used in Figures 3 and 4 to ease

634   comparison, with the dashed line representing the K/Pg boundary.
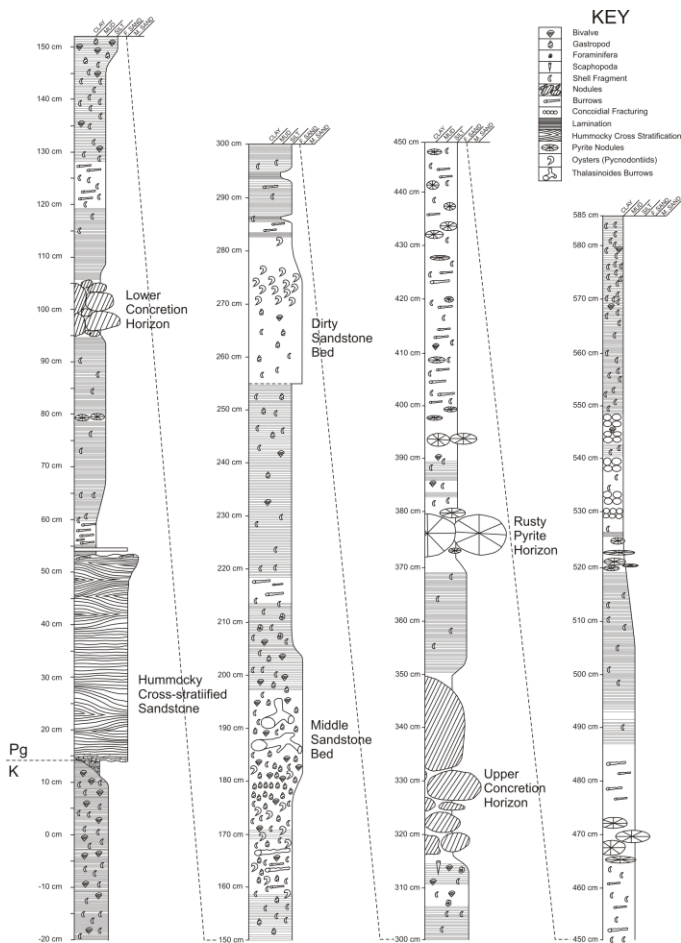
635
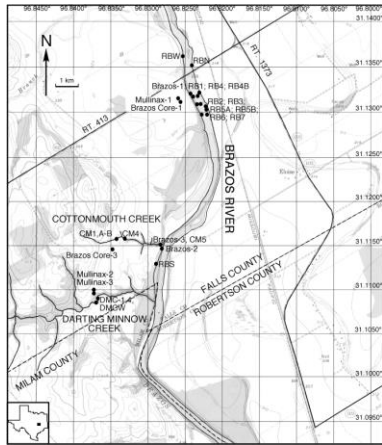
636

637   Figure 1. Locality map of the Brazos River area, Falls County, Texas (after Hart et al., 2012).

638

639

30

640   Figure 2. Sedimentary log of the K/Pg boundary succession exposed on the Brazos River at RBS

641   (based on Hart et al., 2012). The thin volcanic ash recorded in the uppermost Maastrichtian of

642   the Cottonmouth Creek succession (Hart et al., 2012) has not been recorded in the RBS

643   succession, despite digging into the Maastrichtian mudstones as far as river levels allowed.
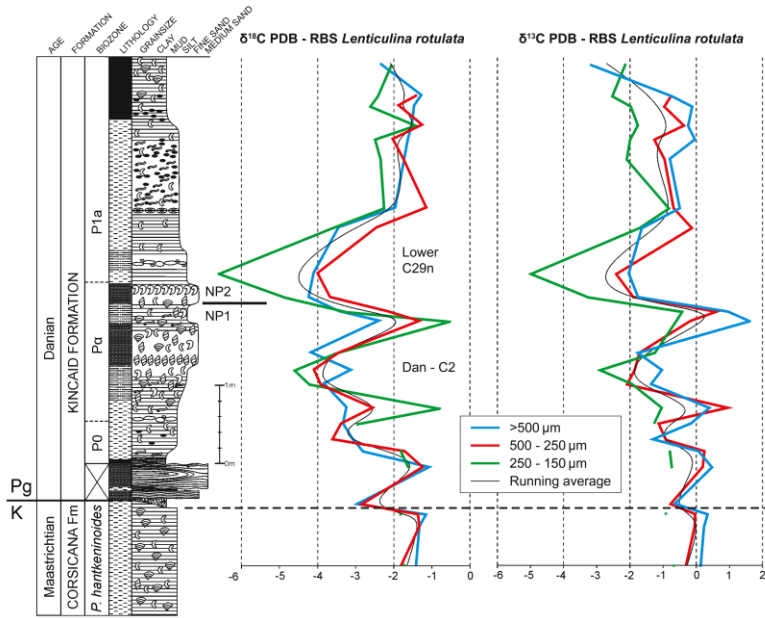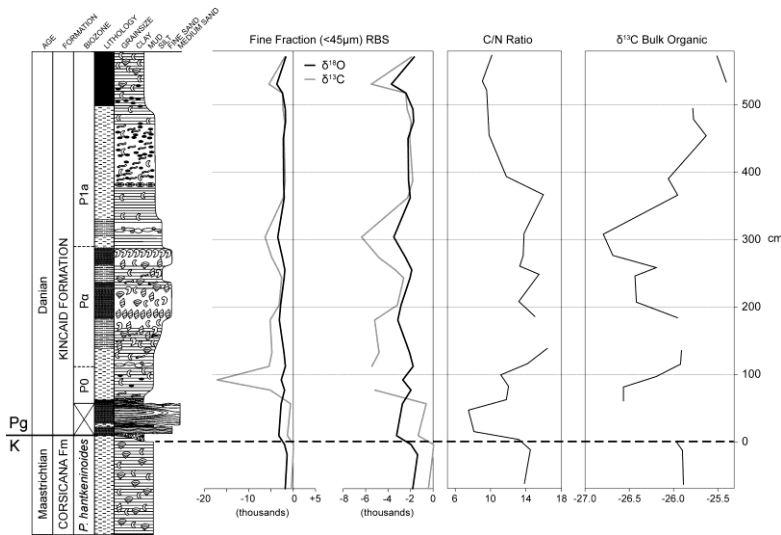
644
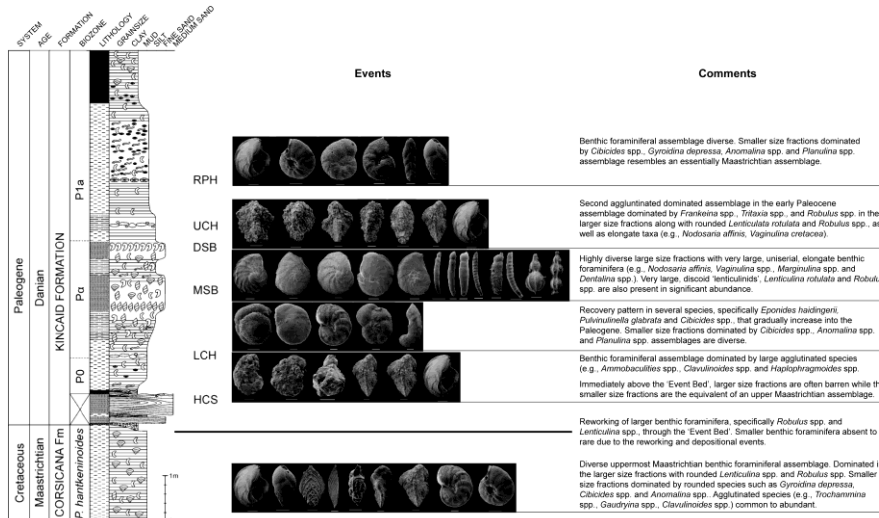
645

646

647   Figure 3. Sedimentary log of the RBS succession, which also shows examples of a representative

648   selection of benthic foraminifera. The lithological symbols are explained in Figure 2 and the bed

649   names follow Yancey (1996) including, from bottom to top, Hummocky Cross-Stratification

650   (HCS), Lower Calcareous Horizon (LCH), Middle Sandstone Bed (MSB), Dirty Sandstone Bed

651   (DSB), Upper Calcareous Horizon (UCH) and Rusty Pyrite Horizon (RPH).

652

653

Figure 4. Comparison of the $\delta^{18}O$ and $\delta^{13}C$ stable isotope data derived from an analysis of

Lenticulina rotulata Lamarck in the >500 µm, 500–250 µm and 250–150 µm size fractions. The

thinner black line marks the running average.

657

Figure 5. Bulk organic $\delta^{13}C$, fine fraction $\delta^{18}O/\delta^{13}C$ and C/N ratio data for the RBS succession.

The data are plotted against the same sedimentary log as used in Figures 3 and 4 to ease

comparison, with the dashed line representing the K/Pg boundary.